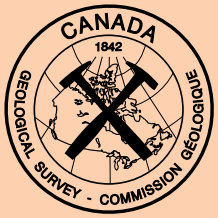

Geological Survey of Canada

CURRENT RESEARCH
2007-A11

Wave dynamics over Roberts Bank, British Columbia: processes and modelling

S. Meulé, P.R. Hill, and C. Pinazo

2007

CURRENT RESEARCH

Natural Resources Canada Ressources naturelles Canada

Canada

ISSN 1701-4387
Catalogue No. M44-2007/A11E-PDF
ISBN 978-0-662-46586-7

A copy of this publication is also available for reference in depository libraries across Canada through access to the Depository Services Program's Web site at http://dsp-psd.pwgsc.gc.ca

A free digital download of this publication is available from GeoPub: http://geopub.nrcan.gc.ca/index_e.php

Toll-free (Canada and U.S.A.): 1-888-252-4301

Critical reviewer
Gwyn Lintern

Authors

S. Meulé
(meule@cerege.fr)
CEREGE, Europôle Méditerranéen de l'Arbois
BP 80, 13545, Aix en Provence
Cedex 04, France

P.R. Hill
(phill@nrcan.gc.ca)
Geological Survey of Canada
9860 West Saanich Road
Sidney, British Columbia
V8L 4B2

C. Pinazo
(christel.pinazo@univmed.fr)
Laboratoire d'océanographie et de Biogéochimie
UMR 6535 CNRS/Université de la Mediterranée
OSU/Centre d'Océanologie de Marseille
Station Marine d'Endoume
Chemin de la Batterie des Lions
13007 Marseille, France

Publication approved by Environment, Safety and Security Portfolio

Correction date:

Wave dynamics over Roberts Bank, British Columbia: processes and modelling

S. Meulé, P.R. Hill, and C. Pinazo

Meulé, S., Hill, P.R., and Pinazo, C., 2007: Wave dynamics over Roberts Bank, British Columbia: processes and modelling; Geological Survey of Canada, Current Research 2007-A11, 9 p.

Abstract: Between 1 March and 26 March 2002, a wave and current measurement station was deployed on the upper delta slope of Roberts Bank in approximately 12 m of water. The field data were analyzed and used in a parabolic wave model to determine wave characteristics for fair-weather, moderate, and storm conditions. The model shows that storm waves act nonuniformly along the beach depending on the local morphology and tidal elevation. Waves propagating during high tide are characterized by smooth dissipation and progressive refraction, whereas waves propagating during low tide show intense refraction and breaking in front of or over a low-tide bar. Sediment transport divergence in the nearshore is strongly controlled by the temporal relationship between storm waves and tidal height.

Résumé : Entre le 1er et le 26 mars 2002, une station instrumentée a été déployée sur la partie supérieure de la pente deltaïque du banc Roberts, dans approximativement 12 m d'eau, afin de mesurer la houle et les courants. Les données de terrain ont été ensuite analysées et utilisées dans un modèle parabolique de houle afin de déterminer les caractéristiques des houles pendant les conditions de beau temps, modérées et de tempête. Le modèle montre que les houles de tempête agissent non uniformément le long de la plage selon la morphologie locale et le marnage. La propagation de la houle à marée haute est caractérisée par une légère dissipation et une réfraction progressive tandis que les houles se propageant à marée basse montrent une intense réfraction et déferlent sur le front ou au-dessus d'une barre de marée basse. La divergence du transport sédimentaire dans la zone littorale est fortement contrôlée par la relation temporelle entre les houles de tempête et le niveau de la marée.

INTRODUCTION

The Fraser River delta is located on the southwest coast of British Columbia. Roberts Bank covers the intertidal delta between the Fraser River main arm channel and Point Roberts headland (Fig. 1). It is important, for planning civil engineering projects and evaluating the ecological sensitivity of deltaic environments, to be able to distinguish areas of active sediment deposition from those characterized by nondeposition and/or erosion. Based on a review of the literature, P.R. Hill (unpub. report, 2001) developed a conceptual model for sediment transport on the delta front, suggesting that erosion in the nearshore of Roberts Bank is related to sediment transport divergence between the outer tidal flats and the delta slope during storms. An objective of the Geoscience for Ocean Management of the Georgia Basin project is to develop tools for evaluating sediment transport issues in the region. This paper reports on field measurements and initial parametric wave propagation model results aimed at understanding the effects of storm events on nearshore sediment transport.

PHYSICAL SETTING

There are two main morphological zones of the subaqueous delta (Hart et al., 1995): the delta front, at the seaward limit of the tidal flat that extends to approximately 10 m depth; and the delta slope, between 10 m and 100 m water depth with a typical slope of 2–3°, but locally reaching 23°, the portion of the delta below the delta front that grades offshore into the prodelta zone (typically <1°). The detailed study area (Fig. 1) was chosen for its linear low-tide shoreline that was interpreted to be highly wave influenced. The local seabed in water depths less than 20 m is characterized by an area of outcropping beds and large, solitary dunes indicating erosional and/or sediment-starved conditions. A LiDAR (Light Detection and Ranging) image, collected on Roberts Bank in 2001, shows an archipelago of small low-tide bars on the outer part of Roberts Bank. Surficial sediment grain size ranges from medium-grained sand on the tidal flat to sandy silt on the lower slope.

Figure 1. Location map showing the study area with instrument deployment site (marked by a tripod symbol) and modelling grid, Roberts Bank, Fraser River delta, British Columbia.

The delta slope is characterized by asymmetric tidal currents with flood dominance. The northwestward-directed flood tidal current attains a maximum speed of 1.3 m/s (Meulé, 2005). The transport of sediment along the delta slope is thus predominantly to the northwest.

In a review of 1967 to 1990 wind data, Hill and Davidson (2002) determined that the most frequent winds are from the east, southeast, and northwest, with the strongest winds blowing from northwest and southeast. The longest fetch is 80 km to the northwest, whereas the fetch from southeast is 45 km. Significant wave heights greater than 1 m occur on average only 6% of the time, whereas heights greater than 0.5 m occur 21% of the time. Storm waves are mainly generated by winds from the southeast and northwest with a small contribution from the south and west.

METHODS

Field measurements and data processing

A Norton instrumented tripod (Birch et al., 2003) was deployed at Roberts Bank in approximately 12 m water depth from 1 to 26 March 2002. Velocity and pressure measurements were recorded with a Marsh McBirney current meter and a Nortek Aquadopp™ Profiler equipped with a pressure gauge. Spectral analysis was used to assess wave characteristics, assuming the sea state to be represented by a superimposition of Airy (sinusoidal) waves (linear approximation). Spectral analysis was conducted on the pressure data using an ensemble and band-averaging power auto spectrum with 512 s Hanning windows and 75% overlap. Pressure measurements were converted to water elevations (Horikawa, 1988), which leads to a necessary cut off imposed at 0.25 Hz. A linear detrending method increased the reliability of the results. Higher cut-off frequencies were also used to evaluate the importance of frequency range. Wave directions were computed using cross-spectral analysis between pressure and velocity time series

Waves in shallow water produce an oscillatory motion. The horizontal orbital velocity is given by the Stokes equation:

$$u = \zeta_0 \bullet \frac{2\pi}{T} \bullet \frac{cosh[k(z+h)]}{sinh[kh]} \bullet \cos(kx - \omega t) + 3\frac{\pi^2}{\lambda T}\zeta_0{}^2 \frac{cosh[2k(z+h)]}{sinh^4[kh]} \bullet \cos 2(kx - \omega t) \quad (1)$$

Where x and z are the horizontal and vertical components, respictively; ς is the sea surface elevation; T is wave period, k is the wave number; h is the water depth; and w is the angular frequency.

The second term of equation 1 represents the wave deformation and is a nonlinear term. When considered negligible (<50 % of the first term), the time-averaged wave orbital motions ($\bar{u}_w = 0$)) were obtained by filtering out the low-frequency velocity fluctuations assumed to be due to the tidal current. When this second term is not negligible, the nearshore wave deformation induces a current. Because this wave-induced current no longer supports the hypothesis, the direction was not calculated. The frequency spread direction was also estimated.

For each burst, the mean water level obtained from the pressure gauge was compared with measurements from the Canadian Hydrographic Service tide gauge located at Point Atkinson, 26 km to the north. Hourly wind speed and direction were obtained from a station at Sand Heads operated by the Canadian Atmospheric Environment Service (Fig. 1).

WAVE PROPAGATION MODEL

The bathymetry of the subtidal portion of the study area was extracted from the GSC multibeam database and rotated to orient the coastline to the top of the grid. The tidal-flat bathymetry was extrapolated using Delaunay linear triangulation.

The propagation of a monochromatic wave is commonly modelled using the mild slope equation:

$$\nabla(CCg\nabla(\phi)) + k^2 CCg\phi = 0 \quad (2)$$

where C is the phase velocity (=ω/k), ω is the wave angular frequency, k is the wave number, ϕ is the horizontal velocity potential, and Cg is group velocity. The elliptic equation of Berkhoff (1972, 1976) was not used in its original form. For computational efficiency, the main direction of wave propagation was projected onto the X-axis and equation 2 was solved in a parabolic form (Radder, 1979):

$$\frac{\partial\phi}{\partial x} = \left(ik\frac{1}{2kCCg}\frac{\partial kCCg}{\partial x}\right)\phi + \frac{i}{2kCCg}\frac{\partial}{\partial y}\left(CCg\frac{\partial\phi}{\partial y}\right) \quad (3)$$

where i is the imaginary number.

Wave information is prescribed only along the upwave boundary of the model. At the other boundaries it is assumed that no waves enter the model. This leads to unrepresentative results near the lateral boundaries. These boundaries must therefore be chosen far enough from the area of interest.

The Radder parabolic equation remains valid for propagation angles within 30° of the initial direction of propagation. Kirby (1986) modified the parabolic equation form to extend the validity to within 50°, whereas Mordane et al. (2004) extended it recently to 90°. From the Kirby (1986) and

Mordane et al. (2004) criterion, equation 3 is valid within 50° for a 10% error; however, this directional restriction implies some limitations on the use of the model.

In the absence of infragravity energy, the breaking criterion, δ, used here is based on Battjes (1974), which defines $\delta = 0.8$ for spilling and plunging waves. When waves break, the surface elevation in the surf zone is recalculated from the equation of Stive (1984):

$$\frac{\partial H}{\partial x} + \frac{H}{4h}\frac{\partial h}{\partial x} = A_{\in}\left(\frac{h}{gT^2}\right)^{\frac{1}{2}}\left(\frac{H}{h}\right)^2 \quad (4)$$

where H is the wave height, h is the depth, $A_{\in}$ is a dimensionless dissipation factor, g is the acceleration due to gravity, and T the wave period. The wave propagation is calculated using an implicit Crank-Nicholson numerical scheme.

FIELD MEASUREMENT RESULTS

The general oceanographic conditions over the study period are shown in Figure 2. The month of measurements included five extended periods of fair-weather conditions and four periods of more energetic conditions including two major storms. The mean water depth shows the mixed semidiurnal tidal oscillation (Fig. 2f). The mean water level was not raised significantly in response to winds and no coastal set up occurred. The spectral energy density plot (Fig. 3) indicates generally low-energy waves mostly confined to the high-frequency range, with most of the recorded periods being under 8 s. Long period waves (>7 s) were associated with small significant wave height generally less than 0.3 m.

Fair-weather conditions (days 1–5, 6–9, 12–15, 17–18, 19–27)

Five periods of fair weather presented similar conditions. Light winds (<10 km/h) occurred for most of the time and they blew from northeast, southeast, and south-southwest. Moderate winds (<20 km/h) blew randomly from the northeast, east-southeast, west-southwest, and north-northwest. Wind direction tended to change abruptly and events lasted only a few hours at a time. These conditions generated waves with significant heights less than 0.25 m coming predominantly from the south, southwest, and northwest. Under these conditions, wave periods were relatively variable, and long wave periods (e.g. 10 s peak period) were recorded on March 2 and March 20.

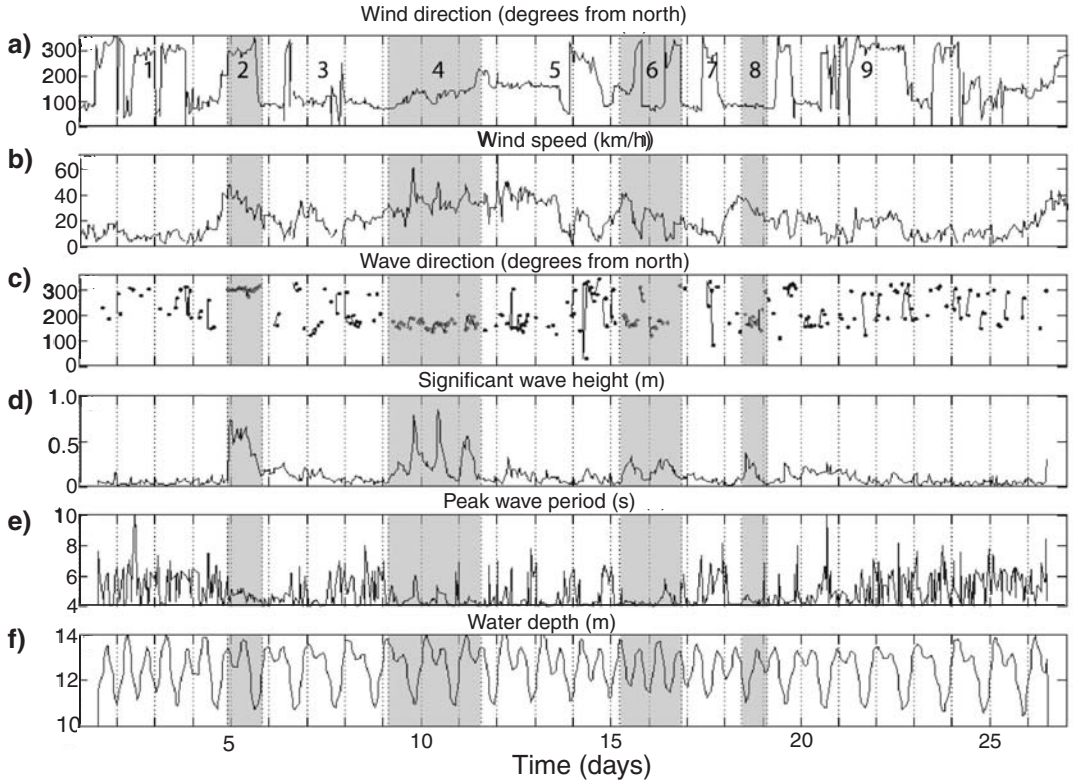

Figure 2. Times series of: **a)** wind direction; **b)** wind speed; **c)** wave direction d**)** significant wave height; **e)** peak wave period; and **f)** mean water depth. The measurement period is divided into different intervals representing fair-weather (1, 3, 5, 7, 9), moderate (6, 8), and major storm conditions (2, 4).

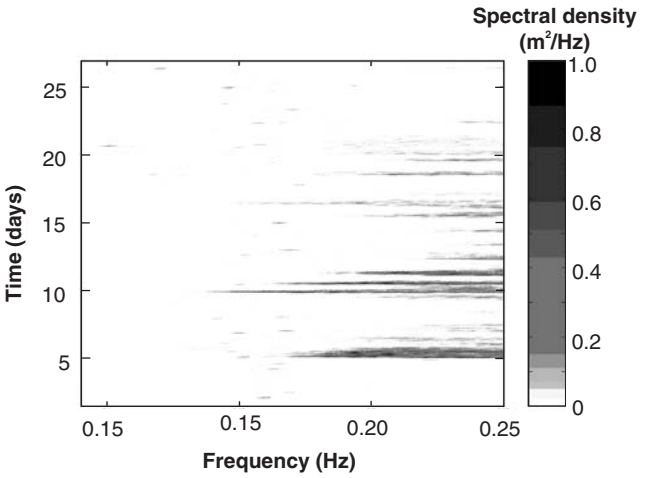

Figure 3. Observed sea-surface spectral density for the period of the study.

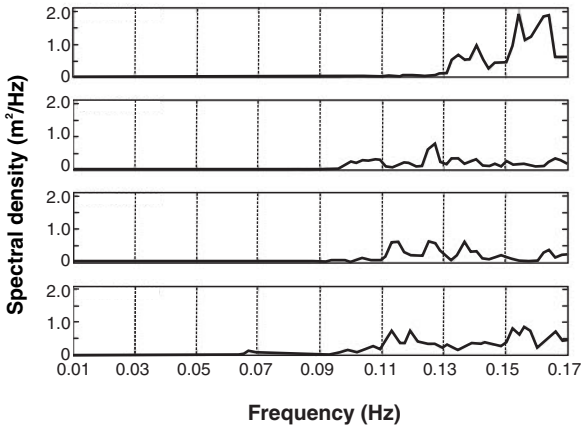

Figure 4. Observed sea-surface spectral density for four selected bursts during the major storm of 5 March 2002.

Moderate storm conditions (days 15–17, 18–19)

Two moderate storm conditions were observed. Wind speeds built overnight and through the end of March 15, reaching 40 km/h. Wind direction switched from the south-east at the peak of the storm to the northwest during the waning storm. Relative small waves with short periods were observed propagating from the south. The significant wave height increased to 0.4 m during a low-tide condition. The energy was confined to the high-frequency range and showed several narrow peaks (below 0.4 m^2/Hz). Wave height decreased during the afternoon of March 15, propagating from the west. After an abrupt easterly rotation of moderate wind speed (30 km/h), the winds switched to the northwest. These conditions during the ebb tide generated moderate waves (Hs: 0.3 m to 0.32 m) associated with both wind directions. They propagated from the south and the south-southeast and were relatively long-period waves, increasing from 4 s to 6 s and then decreasing.

During the second moderate storm, between midday on March 18 to the early morning of March 19, winds blew from the east. Wind speed decreased from 40 km/h to 20 km/h, generating short period waves (between 4.1 s to 4.8 s) from the south, with a maximum significant height of 0.38 m at low tide. Toward the end of the waning phase, wave periods became very variable and very small waves with long periods were recorded. The spectral density distribution was similar to the first moderate storm.

Major storm conditions (days 5 and 9–12)

Day 5 was characterized by a significant storm. As the winds rose through March 4, they turned from the east to the northwest in a clockwise rotation. Winds up to 48 km/h were recorded at the peak of the storm when the water elevation was at the secondary low tide. Significant wave heights exceeded 0.5 m for 12 consecutive hours and reached 0.74 m, propagating from the northwest. Figure 4 displays the spectral density for four bursts over the storm showing the evolution of energy distribution from high-frequency range toward lower frequency. This progression was combined with a progressive loss of energy from 2.1 m^2/Hz when the storm increased suddenly to 0.9 m^2/Hz at the end of the twelfth hour. The peak wave periods ranged between 5.5 s and 4.5 s. As the storm waned, winds rotated back in a counter-clockwise sense to the east. Wave height and period decreased rapidly.

A second intense storm lasted three days between March 9 in the morning and March 11, lasting over two full tidal cycles. Winds switched progressively from the southeast to the southwest over the period of the storm, increasing in speed between 20 km/h and 60 km/h. Three major wind-speed peaks over 50 km/h were observed and corresponded with three peaks of significant wave height (0.77 m, 0.83 m, and 0.55 m). The energy distribution was broad and harmonics were present in the relatively low-frequency range. The first two peak events generated relatively long period waves (6 s and 5.4 s), whereas the last peak event of this storm was associated with short period wave (4.6 s). Waves came predominantly from the south and south-southeast. Waves for the first peak propagated during low tide, whereas the two later peaks were at high tide.

MODEL SIMULATIONS

Figure 5 presents the bathymetric grid used for wave simulation. The colour scale highlights the main features in shallow water. The upper shoreface slope breaks between 6 m and 7 m water depth. Above this depth, the morphology is characterized by the presence of a low-tide bar and trough system

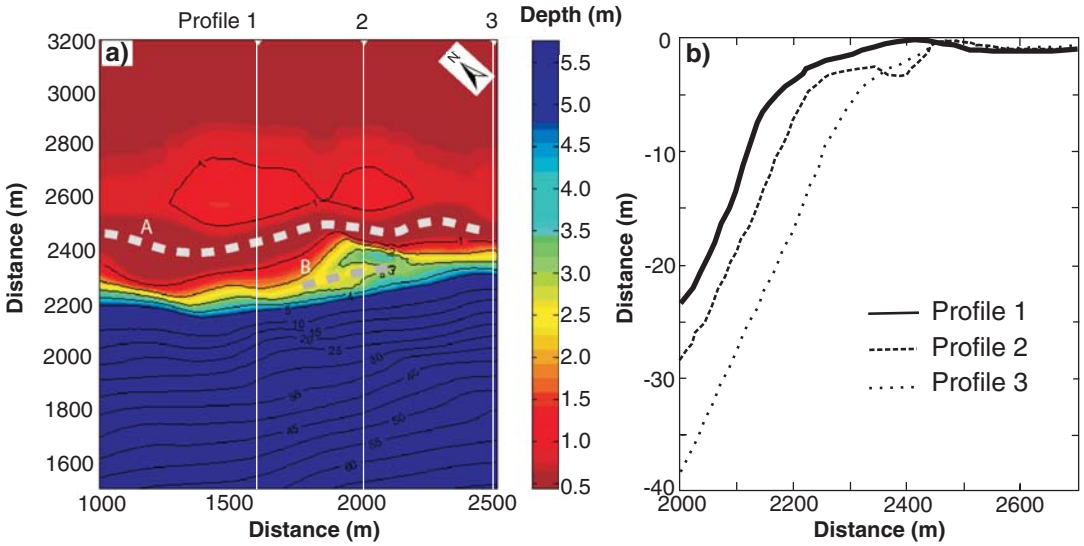

Figure 5. a) Bathymetric grid used for wave simulation. The three cross-shore profiles shown in Figure 5b are indicated by the white lines. The three upside-down triangles indicate the position of cross-shore profile. **b)** Cross-shore bathymetric profiles; profile 1 shows only the low-tide bar; profile 2 shows the outer bar and low-tide bar; profile 3 shows no bars.

Table 1. Wave parameters for simulation. Conditions were chosen to represent fair-weather and both moderate-storm and major storm conditions.

Figure	Condition	Time (h)	Wave height (m)	Peak wave period (s)	Wave incidence (degrees from north)	Tidal elevation (m)
N/A	Fair-weather	03 March 11:00	0.03	7.31	243	1.25
6a	First moderate storm	15 March 13:00	0.33	4.26	197	1.30
6b	Second moderate storm	16 March 12:00	0.30	5.12	261	1.18
7	Second major storm	10 March 12:00	0.84	5.06	181	2.46
8	Second major storm	09 March 20:00	0.78	5.39	215	0.53
9	Second major storm	09 March 20:00	0.78	5.39	215	0.53

almost parallel to the shoreline in about 2 m of water (A, Fig. 5). At the northern side of the domain, the height of the bar is about 1.3 m and the width is about 250 m. The low-tide bar progressively disappears southward. A broad trough separates the low-tide bar from the tidal flat. A second parallel bar, with a crest depth of 3 m, is located in the central part of the grid (B, Fig. 5). The height of the bar is less than 1 m and the width is about 100 m. This low-amplitude ridge is almost 300 m long and is slightly oblique to the shoreline. Wave parameters from the field measurements were used as input parameters for 2-D simulation. The wave conditions outlined in Table 1 were chosen to represent fair-weather, moderate, and storm conditions. The tide elevation measured with a Marsh McBirney pressure gauge was considered in each simulation.

Fair-weather conditions

Wave heights were almost insignificant during fair-weather periods. Very small waves from all directions propagate across the upper shoreface without any modification. The effect of wave breaking is negligible, but the low tide bar induced a few centimetres of shoaling in very shallow water. Waves converge over the front of the bar and diverge on the lee side.

Moderate storm conditions

Figure 6 shows the pattern of the significant wave height for the moderate storm conditions. The two simulations show similar characteristics despite the two different wave incident angles (Table 1). On the tidal flat, a noisy amplitude modulation spreads across the model grid suggesting that the Radder parabolic approximation is no longer valid in these extremely shallow water depths; however, these cases provide useful information in deep water.

In the first simulation (Fig. 6a), at low tide (1.30 m), waves propagate from the south with near-normal incidence. Significant refraction begins in water depths between 1 m and 2 m. Incident waves remain unmodified over the outer bar. Over the low-tide bar, wave heights increase when refraction

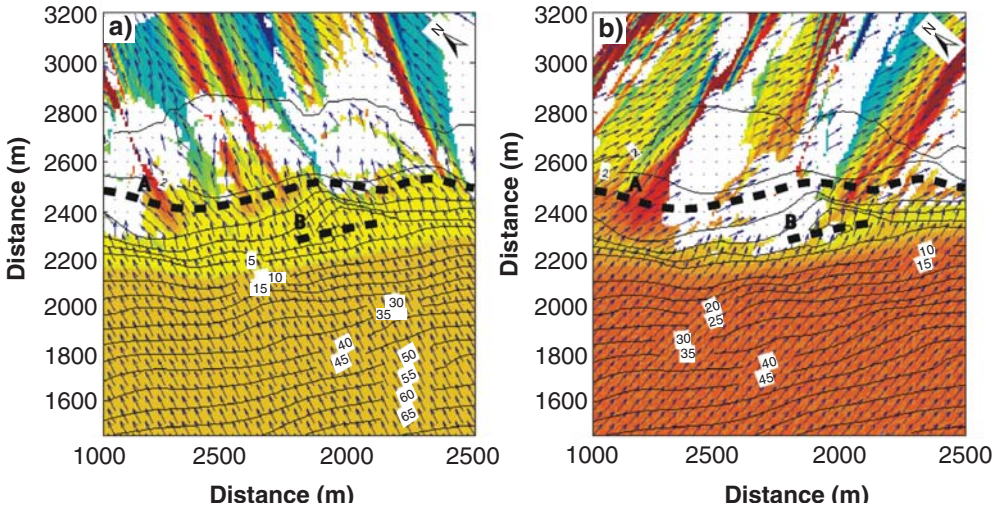

Figure 6. Wave-height simulation during **a)** the first moderate storm condition and **b)** during the second moderate storm condition (*see* Table 1 for parameters). Arrows indicate direction of propagation. Oblique bands of colour on the tidal flats indicate amplitude modulation, suggesting that the Radder parabolic approximation of equation 3 is no longer valid. Blank areas indicate invalid data where the refraction angle exceeds 50° from the original direction. Depth contours are referenced to the actual sea level of the simulated period, taking into account the tide. The bar crests (A and B as in Fig. 5) are indicated by dashed lines.

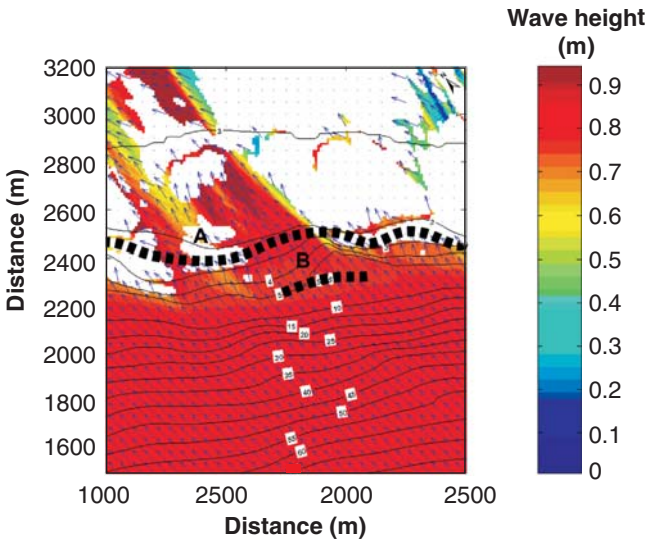

Figure 7. Wave - height simulation during the second major storm condition (*see* Table 1 for parameters). Arrows indicate direction of propagation. Oblique bands of colour on the tidal flats indicate amplitude modulation suggesting that the Radder parabolic approximation of equation 3 is no longer valid. Blank areas indicate invalid data where the refraction angle exceeds 50° from the original direction. Depth contours are referenced to the actual sea level of the simulated period, taking into account the tide. The bar crests (A and B as in Fig. 5) are indicated by dashed lines.

causes focusing of wave energy (convergence) and decrease when refraction causes spreading of energy (divergence). No wave breaking occurs.

In the second simulation (Fig. 6b), also at low tide (1.18 m), the angle of incidence is greater and waves refract northward over the outer bar, creating a nonvalid area in shallow water behind it due to angle limitation. A slight clockwise refraction in the north and a slight counter-clockwise refraction in the south create a general convergence of waves over the inner bar. The gradual increase of wave height over the bar is due to shoaling processes. Waves do not break on the bar, but may break on the tidal flat; however, the amplitude modulation generated by the simulation over the tidal flat prevents direct observation of this.

Major storm conditions

The first storm was impossible to simulate because the wave direction was almost parallel to the shoreline. The simulations of major storm conditions were therefore based on conditions from the second storm on 9–10 March. Figure 7 shows a simulation for a 0.83 m incident wave height at a tide height of 2.46 m during the flood phase of a secondary high tide. In areas where the incident direction is more oblique to the bathymetric contours, refraction generates large patches of nonvalid results due to the angle limitation. Where valid

results were obtained, wave transformations can be inferred. Waves from the south start to refract and shoal at a depth between 4 m and 5 m, in this case inside the outer bar (B). The presence of subtle areas of decreased wave height (indicated by lightening of the red tone on Fig. 7) suggests partial wave breaking over both bars, but a large proportion of the wave energy propagates onto the tidal flats.

Figure 8 shows a simulation for a 0.78 m incident wave height propagating from the southwest during low tide (0.53 m). The pattern of wave transformation is very different from the high-tide simulation. Over the outer bar (B), decreased wave heights indicate significant, but incomplete wave breaking. As the waves approach the inner bar (A), increased height inside the 2 m isobath followed by an even more significant decrease inside the 1 m isobath indicate shoaling and breaking along the inner bar. These transformations are shown along a single transect in Figure 9. Wave heights remain below 0.4 m across the tidal flats.

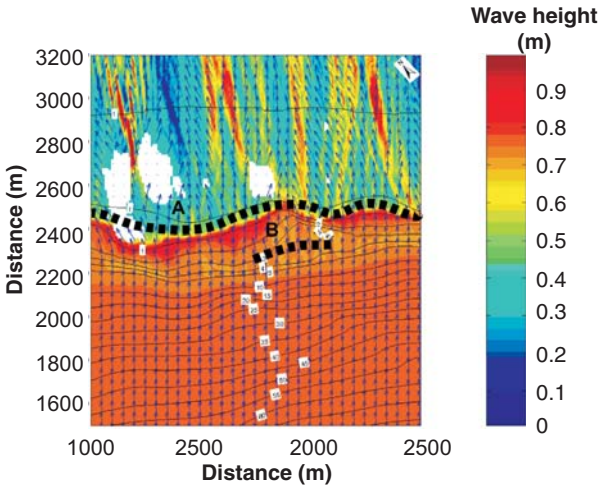

Figure 8. Wave-height simulation during the second major storm condition (*see* Table 1 for parameters). Arrows indicate direction of propagation. Oblique bands of colour on the tidal flats indicate amplitude modulation, suggesting that the Radder parabolic approximation of equation 3 is no longer valid. Blank areas indicate invalid data where the refraction angle exceeds 50° from the original direction. Depth contours are referenced to the actual sea level of the simulated period, taking into account the tide. The

DISCUSSION

During the field measurements, the winds blew for the longest duration from the southeast where the fetch is limited. Waves were predominantly short period, indicating that they were directly wind-induced and did not have swell or infragravity wave components. When winds rotated from south to west, the recorded waves were higher and of longer period; however, wave heights remained below 1 m. Thomson (1981) and Luternauer et al. (1998) calculated that wave heights could exceed 1.2 m for 10% of the year.

The main limitation of the model in this setting is the high angle of refractions due to the extreme shallow water of the tidal flat at low tide, making wave parameters fall outside of the valid model domain. Also wave and/or current interactions were not considered. Although tidal currents are particularly strong in this area, most of the storm wave peaks in the field measurements occurred coincidently at low tide when the tidal currents were minimal. Furthermore, wave directions were measured in 12 m of water, at which depth the waves may already be refracted by the tidal current. In this sense the simulations are valid for the observed conditions, but wave and/or current interactions would more typically be an important consideration. The model runs show an initial gradual decrease of wave height associated with slight refraction in the upper shoreface. Whereas the validity of equation 2 could also be called into question, given the higher slope gradient for the mid-slope equation, wave heights decrease by only a few centimetres and are almost negligible.

The model shows that due to the nearshore slope and morphology, waves act nonuniformly along the shore. As waves propagate into shallow water, wave heights and wavelengths change in response to shoaling and refraction. Oscillatory wave motions become significant under moderate storms at a depth between 4 m and 6 m. Nielsen (1992) estimated a practical depth of closure as 3.5 times the annual maximum significant wave height (Hs) beyond which changes are insignificant. Assuming values of wave height between 1.3 m and a maximum of 3.1 m (Thomson, 1981), the upper shoreface slope break coincide with this water depth (*see* Fig. 5b).

The behaviour of waves after this point depends on the tide elevation, incident wave angle, and the bottom topography. At high tide, small waves propagate into shallow water

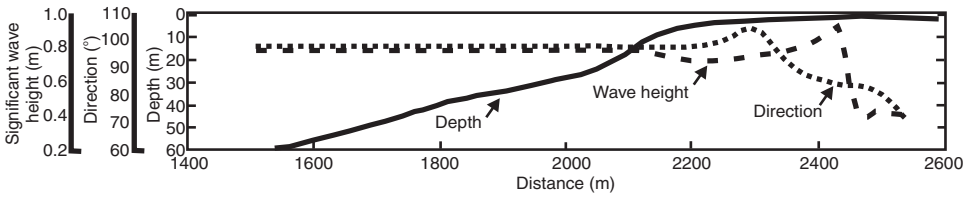

Figure 9. Cross-shore profile at a distance of 2250 m on the x-axis of Figure 8, superimposing wave-height simulation, wave-direction simulation, and bathymetry during the second major storm at low tide (*see* Table 1 for parameters).

without any modification. Larger waves refract slowly over the relatively gentle slope and wave energy is progressively dissipated in the shallower water. At low tide, the upper beach is very steep and nondissipative. When waves propagate into shallow water, oscillatory motions become important on the upper slope. Waves refract over a short distance without shoaling and abruptly break over the inner bar. Calculations suggest breaking would be in the form of a spilling wave. These large variations in significant wave height imply large variations in the spectral energy distribution.

Wave dissipation due to refraction and breaking provides the energy for sediment transport. The focus of this energy depends on the temporal relationship between tide height, bathymetry, and wave height. With the particular bathymetry of this deltaic environment, characterized by a steep slope followed by a shallow, low-angle tidal flat the spatial distribution of wave energy due to refraction and breaking varies drastically with the tide height. At high tide, wave energy is more evenly distributed across the tidal flat, whereas, at low tide, the wave energy is highly concentrated at the top of the slope. The relative importance of these temporally modulated conditions will determine net sediment transport on the shoreface.

CONCLUSIONS

- For the period of the field measurements on the upper slope of the Fraser River delta, waves were predominantly wind-induced and did not have swell or infragravity wave components. When winds rotated from south to west, the recorded waves were higher and of longer period; however, wave heights remained below1 m.
- The behaviour of waves after the upper shoreface slope break depends on the tide elevation, incident wave angle and the bottom topography. At high tide, waves refract slowly over the relatively gentle slope. At low tide, the upper beach is very steep and waves refract over a short distance without shoaling and may abruptly break in front of or over a low-tide bar.
- Sediment transport in the nearshore will be strongly controlled by the temporal relationship between storm waves and tidal height.

REFERENCES

Battjes, J.A.
1974: Surf similarity; *in* Proceedings, 14th International Coastal Engineering Conference, Copenhagen, Denmark, June 24–28, 1974, American Society of Civil Engineers, p. 446–480.

Berkhoff, J.C.W.
1972: Computation of combined refraction-diffraction; *in* Proceedings, 13th International Conference on Coastal Engineering, Vancouver, British Columbia, July 10–14, 1972, American Society of Civil Engineers, p. 741–790.

Mathematical models for simple harmonic linear water waves; wave diffraction and refraction; Doctoral thesis, Delft University of Technology, Delft, Netherlands, 103 p.

Birch, R., Hill, P.R., Clarke, M., Lemon, D., and Fissel, D.
2003: A configurable multi-sensor tripod for the study of near-bottom ocean processes; *in* Oceans 2003, San Diego, California, September 22–26, 2003, Institute of Electrical and Electronics Engineers, v. 4, p. 2254–2260.

Hart, B.S., Hamilton, T.S., Prior, D.B., and Barrie, J.V.
1995: Seismostratigraphy and sedimentary framework of a deep water Holocene delta: Fraser River, British Columbia; *in* Geology of Deltas, (ed.) M.N. Oti and G. Postma; Balkema, A.A.: Rotterdam, Netherlands, p. 167–178.

Hill, P.R. and Davidson, S.
2002: Preliminary modeling of sediment transport on the upper foreslope of the Fraser River delta; Geological Survey of Canada, Current Research 2002-E2, 9 p.

Horikawa, K.
1988: Nearshore Dynamics and Coastal Processes: Theory, Measurement and Predictive Models; University of Tokyo Press, Tokyo, Japan, 522 p.

Kirby, J.T.
1986: Higher approximations in the parabolic equation method for water waves; Journal of Geophysical Research, v. 91, p. 933–952.

Luternauer, J.L., Mosher, D.C., Clague, J.J., and Atkins, R.J.
1998: Sedimentary environments of the Fraser delta; *in* Geology and Natural Hazards of the Fraser River Delta, British Columbia (ed.) J.J. Clague, J.L. Luternauer, and D.C. Mosher; Geological Survey of Canada, Bulletin 525, p. 27–39.

Meulé, S.
2005: Processus mis en jeu dans l'évolution morpho-dynamique de Roberts Bank (Delta du Fraser) : Observation et modélisation hydrodynamiques et sédimentaires; Ph.D. thesis, Université du Québec à Rimouski, Rimouski, Quebec, 156 p. and Appendices.

Mordane, S., Mangoub, G., Maroihi, K.L., and Chagdali, M.
2004: A parabolic equation based on a rational quadratic approximation for surface gravity wave propagation; Coastal Engineering, v. 50. p. 85–95.

Nielsen, P.
1992: Coastal Bottom Boundary Layers and Sediment Transport; World Scientific Publishing Company Ltd., Singapore, 340 p.

Radder, A.C.
1979: On the parabolic equation method for water wave propagating method; Journal of Fluid Mechanics, v. 95, p. 159–176.

Stive, M.J.F.
1984: Energy dissipation in waves breaking on gentle slopes; Coastal Engineering, v. 8, p. 99–127.

Thomson, R.
1981: The oceanography of the British Columbia coast; Canadian Special Publication of Fisheries and Aquatic Sciences, Ottawa, Ontario, Department of Fisheries, Bulletin 56, 291 p.

Geological Survey of Canada Project X43